Investigation into Potential Modal Coupling in a Bolted Structure Using a Nonlinear ROM and QSMA

Daniel Agramonte[1*], Gabrielle Graves[2*], Kenneth Meyer[3*], Ben Pacini[4*], Dan Roettgen[4], Matt Allen[4], Moheimin Khan[4], David Najera-Flores[4] and Aabhas Singh[4]

[1]The College of Engineering The University of Georgia,130 Riverbend Rd, Athens, 30603, Georgia, United States.
[2]School of Engineering The University of New Mexico 210 University Blvd NE, Albuquerque, 87106, New Mexico, United States.
[3]Cockrell School of Engineering, The University of Texas at Austin, 301 E. Dean Keeton St. C2100, Austin, 78712-2100, Texas, United States.
[4]Sandia National Laboratories†, P.O. Box 5800, Albuquerque, 87185, New Mexico, United States.

*Corresponding author(s). E-mail(s): dn.agramonte@gmail.com; gabriellegraves2016@gmail.com; kmeyer299@gmail.com; brpacin@sandia.gov;

Abstract

Jointed interfaces are sources of nonlinearity within a structure and typically demonstrate an increase in damping and reduced stiffness at high excitation levels. According to some constitutive models, the damping

†Sandia National Laboratories is a multimission laboratory managed and operated by National Technology and Engineering Solutions of Sandia, LLC., a wholly owned subsidiary of Honeywell International, Inc., for the U.S. Department of Energy's National Nuclear Security Administration under contract DE-NA-0003525.

will then begin to decrease with further increases in system energy. This work investigates a structure in a fixed-free boundary condition that exhibited this behavior in previous experiments. In the present study, modal coupling is examined to determine if it is the cause of this behavior and not the physics of the jointed interface. This initial investigation utilizes nonlinear experimental techniques along with nonlinear reduced order modeling and quasi-static modal analysis to determine if these modeling approaches can capture the potential modal coupling effects.

Keywords: Nonlinear Dynamics, Modal Coupling, Reduced Order Modeling, QSMA

1 Introduction

Bolted joints are common in structures due to the ease of assembly and disassembly and the impracticality of manufacturing monolithic structures. Despite their common use in structures, they are often approximated using linear dampers or even ignored [1]. This is, in part, due to the complex physics of jointed interfaces and the uncertainties due to the nonlinearities. Common linear analysis may be sufficient for weakly nonlinear structures at low amplitude levels, but they do not capture the complex properties and dynamics at higher forcing amplitudes.

Bolted joints typically cause nonlinear damping and nonlinear softening of each affected mode in a structure during the micro-slip regime. These behaviors have been specifically seen in cantilever beams such as the Brake-Reuß beam with a lap joint and the S4 beam [2] as well as more complex structures such as the BARC system [3] and others [4, 5]. Various modeling techniques have been proposed to capture the hysteretic properties of joints; some of those used in this work include the Iwan model and the modal Iwan model [6, 7]. The latter is more straightforward to apply, but it captures the energy dissipation in a modal space, so coupling between modes is difficult to account for. In contrast, a discrete Iwan model can be placed at the actual interface in a model and has the possibility of capturing mode coupling and the nonlinear properties of each mode, as done in [8], although the ability of this approach to capture mode coupling has not been studied in detail.

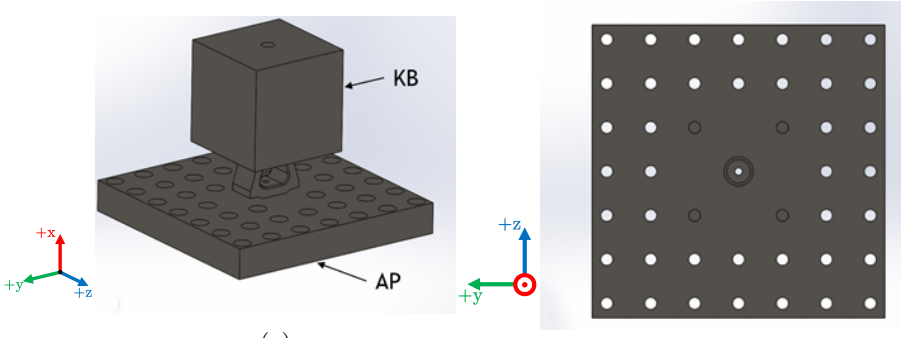

(a) (b)

Fig. 1: (a) shows an isometric view of the bolted structure, which consists of a Kettlebell (KB) and Adapter Plate (AP), and (b) shows a bottom view of the bolted structure [9]

This work builds of a previous study conducted by Khan et al. [9] as a part of the 2021 Nonlinear Mechanics and Dynamics (NOMAD) Summer Research Institute. In the work by Khan et al., a structure was devised such that the 1st axial mode in x ($r = 5$ with r denoting mode number) will exert

a large alternating stress on the bolt connecting the Kettlebell (KB) and the Adaptor Plate (AP) as seen in Figure 1.

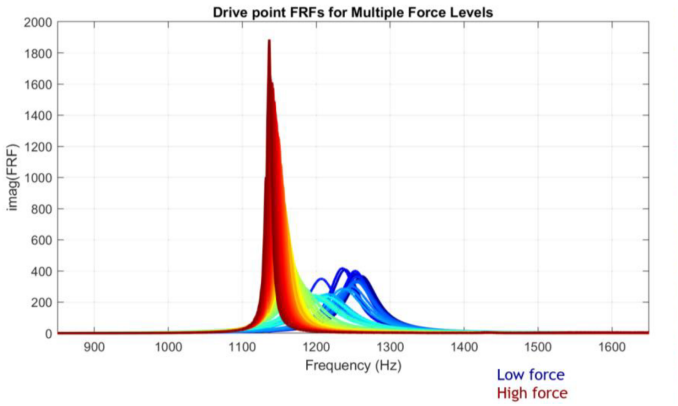

Fig. 2: Drive Point FRF for various forcing levels in the axial mode [9]

In Khan et al. [9], a series of band limited random excitation experiments were conducted at various excitation amplitudes. The excitation bandwidth encompassed the 1st axial mode in x (Mode 5) and 2nd bending mode in y (Mode 4) of the system. Additionally, the excitation degree of freedom (DOF) was selected to primarily drive the response of Mode 5 and minimally excite all other modes. At large forcing amplitudes, the apparent damping of Mode 5 drastically decreased and the natural frequency of the axial mode softened and converged to that of Mode 4 as demonstrated in Figure 2. Furthermore, the work in [9] showed clearly that the response of Mode 4 increased in proportion of the total response as the excitation increased. This indicated the potential that Modes 4 and 5 were coupled, thus motivating the present study as an initial investigation to understand this behavior.

The approach taken in this work to study this potential coupling utilizes a combination of experimental and analytical techniques. After a brief introduction to modal coupling (Section 2), Section 3 describes the experimental set-up and data processing used to extract linear modal properties along with amplitude-dependent natural frequency and damping trends for Modes 4 and 5. These data are used by the two analytical techniques utilized in this work: Quasi-Static Modal Analysis (QSMA) [8] and nonlinear reduced order modeling (ROM). Sections 4 and 5, respectively, discuss the model updating efforts as well as the capability of each method to capture the potential coupling of the modes of interest. Section 6 provides conclusions from this initial study of the complex nature of modal coupling.

2 Modal Coupling

The general, nonlinear, N degree of freedom (DOF) equation of motion (EOM) may be written as follows.

$$\mathbf{M}\ddot{\mathbf{x}} + \mathbf{C}\dot{\mathbf{x}} + \mathbf{K}\mathbf{x} + \mathbf{f}_{NL}(\mathbf{x}, \dot{\mathbf{x}}) = \mathbf{f}(t) \tag{1}$$

With some assumptions [2], we may simplify Equation 1 to N coupled equations in modal space

$$\ddot{q}_r + 2\zeta_r(\mathbf{Q})\omega_r(\mathbf{Q})\dot{q} + \omega_r^2(\mathbf{Q})q_r = \boldsymbol{\phi}_r \boldsymbol{f}(t), \tag{2}$$

where $\mathbf{Q} \in \mathbb{R}^N$ is the vector of modal amplitudes and ζ_r, $\omega_r : \mathbb{R}^N \mapsto \mathbb{R}$. Equation 2 shows that the response of mode r is depended on the response of the other modes in $\mathbf{Q}$. This is referred to as modal coupling. If the system has negligible modal coupling, then we say that $\zeta_r(\mathbf{Q}) \approx \zeta_r(Q_r)$ and $\omega_r(\mathbf{Q}) \approx \omega_r(Q_r)$.

3 Experimental Data and Analysis

3.1 Test Set Up

Both linear and nonlinear system identification techniques were used to evaluate the modal coupling and provide data for the QSMA and nonlinear ROM. Low-level (linear) and high-level (nonlinear) fixed-base impact testing was performed on the assembly with the AP bolted to a large seismic mass as seen in Figure 3b.

The 11 accelerometer and 3 drive point locations are shown in Figure 3c. Node 1001 would excite primarily the 1$^{\text{st}}$ axial mode in x (Mode 5), node 1002 would excite both modes, and node 1003 would excite primarily the 2$^{\text{nd}}$ bending mode in y (Mode 4). Additionally, during initial assembly prior to testing in [9], a force-sensing bolt was used to attach the KB to the AP, allowing for the determination of the clamping force provided by the bolt. During this initial assembly, this bolt was torqued such that a preload of 2027 lb_f was applied. The KB and AP remained assembled from this initial assembly and throughout the entirety of the testing discussed here. The KB-AP assembly was attached to a seismic mass to create a fixed-free boundary condition.

3.2 Linear Testing

Impact testing using low-level forces ($<5\text{lb}_\text{f}$ peak) with a hammer was conducted and frequency response functions (FRF's) were computed from the measured data. Natural frequencies, damping ratios, and mode shapes were extracted from these set of FRFs and are recorded in Table 1.

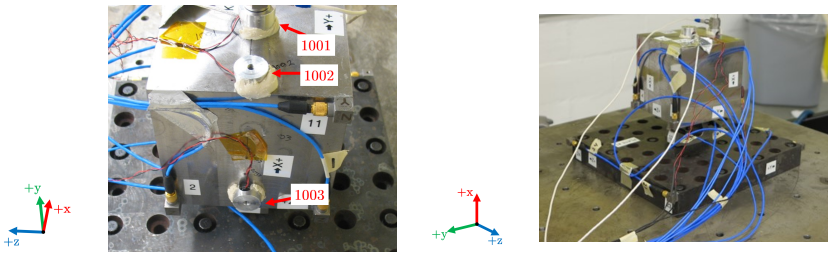

(a) (b)

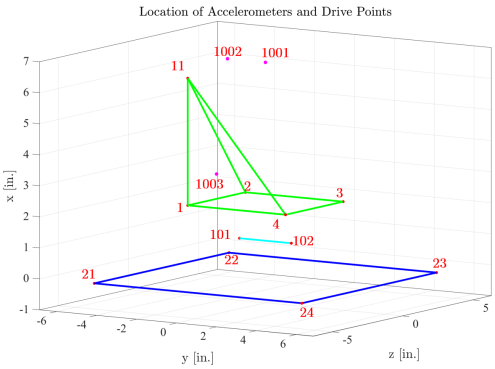

(c)

Fig. 3: (a) Close up view of the drive points. (b) Experimental set up with seismic mass. (c) Location of all accelerometers and drive points

Table 1: Experimentally Measured Linear Modal Parameters

Mode	Description	Frequency [Hz]	Damping
1	1^{st} bending in z	101.5	0.01072
2	1^{st} bending in y	178.9	0.00423
3	1^{st} torsion about x	348.1	0.00402
4	2^{nd} bending in y	1137.3	0.00045
5	1^{st} axial in x	1182.2	0.00266
6	2^{nd} bending in z	1469.0	0.00290

3.3 Nonlinear Testing

High level hammer testing (10-80 lb_f peak) was then conducted at the three drive points shown in Figure 3c. The amplitude dependent frequency and damping curves for Modes 4 and 5 were extracted from these data using the method from [10] . This method first uses the linear mode shapes and band pass filtering to extract the individual modal responses from the measured data. A

Hilbert transform [11] is then utilized to approximate the decay envelope and instantaneous phase of each modal time response. The instantaneous damping coefficient and damped frequency were then determined from these curves [10].

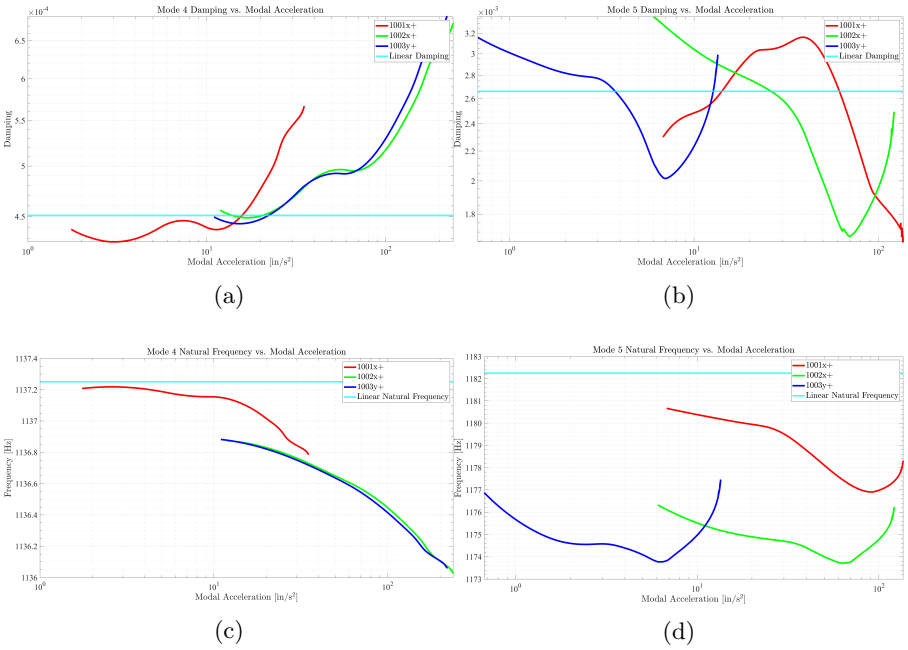

Fig. 4: Amplitude dependent frequency and damping curves for Mode 4 ((a),(c) the 2$^{\text{nd}}$ bending mode in y) and Mode 5 ((b),(d) the 1$^{\text{st}}$ axial mode in x).

Figure 4 shows the amplitude dependent natural frequency and damping for Modes 4 and 5 extracted from the experiments at each of the three drive points. These results indicate that there is one way coupling between Mode 5 and Mode 4, but not between 4 and 5. Specifically, Mode 4 shows the same behavior from all three drive points, and drive points 1001x+ and 1002x+ excite it together with Mode 5. In contrast, the behavior of Mode 5 is seen to depend strongly on drive point. We would presume that the data from the 1001x+ drive point (red) is the behavior that Mode 5 would have in isolation and that the other curves deviate because Mode 4 is also excited in those responses. The following sections describe efforts to date to model this system.

4 QSMA

QSMA is a method that applies a monotonically increasing load to a finite element model (FEM) in the shape of a mode of interest [8]. QSMA

can be used to determine the nonlinear stiffness and damping that arise from the bolted interfaces [8]. Specifically, the nonlinearities are characterized by a hysteresis curve that is formed by applying a force in the shape of the mode of interest. The amplitude-dependent stiffness is the secant of the hysteresis' backbone curve and the amplitude-dependent damping is proportional to the area enclosed or the energy dissipated in one cycle.

When using modal models to characterize a nonlinear structure, modal coupling is revealed when the effective frequency or damping of a mode is found to change as the amplitudes of other modes are varied. Singh et al. [12] recently extended QSMA to estimate this effect by applying loads in the shape of multiple modes simultaneously. A similar method is applied here to determine if the model with QSMA can replicate the trends seen in Section 3.3.

Although QSMA is less computationally expensive than direct time integration of a FEM when determining the nonlinear characteristics of a system, the method does require certain components and properties in a finite element model (FEM). For bolted structures, the preload and the interface friction properties must be defined. The nonlinear FEM model that was used for the QSMA was created using Abaqus CAE. Unlike the reduced-order model (see Section 5), the bolt, nut, and washers were all included in the FEM. These components were modeled with 3D elements with an applied preload of 2025 lb_f to capture the clamping force in the bolts. The FEM was composed of standard linear tetrahedral elements to model the adapter plate and quadratic tetrahedral elements for the kettlebell structure.

Section 4.1 discusses the validation of the linear model used as the baseline for the nonlinear FEM implemented in the QSMA and its comparison to the corresponding measured results from Section 3.2. The results of the QSMA is conducted in Section 4.2.

4.1 Linear Model Creation for QSMA

Before performing QSMA, a linear modal analysis was conducted on the finite element model to verify the likeness of the natural frequencies and mode shapes to the first six modes of vibration that were measured on the structure. Table 2 shows the natural frequencies calculated in Abaqus and the error between the simulated and experimental frequencies.

The higher modes of vibration have a much lower error than the first and second modes. During experimental modal testing it was noted that Mode 5, the first axial mode, did not involve pure axial motion but exhibited a slight tilt in y. The geometry and contact interface were symmetric in the FEM, and so it could not capture this effect. Figure 5 shows FEA mode shapes for Modes 4 and 5. After determining the natural frequencies, the modal assurance criterion (MAC) [13, 14] was calculated to compare the simulated and experimental mode shapes for each mode of interest. The MAC values were all close to 1.0, with the lowest values occurring for Mode 1, which had $\text{MAC}_{11} = 0.93$.

Table 2: Natural Frequencies in Abaqus Model

Mode	Experimental (Truth) [Hz]	Model [Hz]	Error [%]
1st Bending in z	101.5	124.21	22.4
1st Bending in y	178.9	186.48	4.2
1st Torsion about x	348.1	383.45	10.2
2nd Bending in y	1137.3	1143.5	0.6
1st Axial in x	1182.2	1255.2	6.2
2nd Bending in z	1469.0	1542.6	5.0
		max|% Error|	22.4
		$\sum$|% Error|/6	8.1

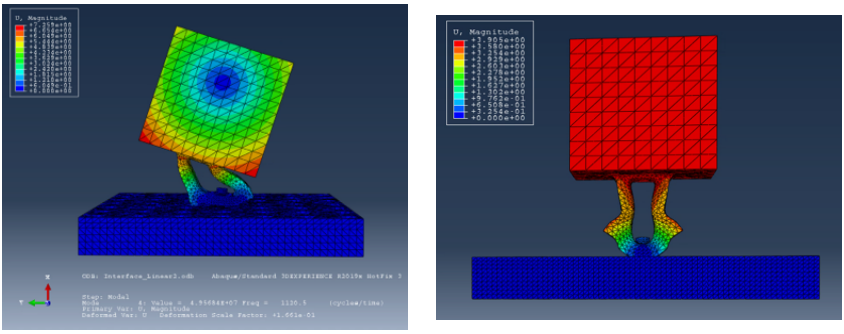

(a) (b)

Fig. 5: Mode shapes from FEM for (a) Mode 4, 2nd Bending mode in y, and (b) Mode 5, 1st axial mode in x

4.2 QSMA Results

QSMA was conducted on the model to determine the nonlinear characteristics of the structure and evaluate the potential coupling between Modes 4 and 5, see Figure 6. It should be noted that the response amplitudes from QSMA seen for both modes are significantly higher than those achieved in the experiments. As such, only the trends of the data are discussed. QSMA predicts hardening behavior (i.e. increase in frequency with amplitude) for Mode 4 which conflicts with the corresponding experimental results. This resulted in a non-physical damping curve in the QSMA analysis and as such is not shown here. For Mode 5, the QSMA results show a softening behavior which agrees with the experimental results. However, QSMA predicts the damping for this mode to increase whereas the experimental data showed a decrease in this parameter as response amplitude increases. To seek to understand these discrepancies, the stick-slip behavior and the pressure distribution of both modes were analyzed.

When a bolted structure slips at the joint interface, the area that is stuck decreases, reducing the amount of area that contributes to the overall stiffness, thus reducing the effective stiffness. Therefore, the change in the stick and slip regions at the joint interface as the quasi-static load increases will indicate changes in the natural frequency. The pressure distribution and the stick-slip conditions computed during the QSMA for Modes 4 and 5 were investigated. For a half cycle of loading, Mode 5 was seen to have a decreasing pressure area, consistent with the reduced natural frequency seen in Figure 6. However, the pressure area for Mode 4 was shown to increase, causing a corresponding increase its the natural frequency in the QSMA. The experimental results for this mode indicate a softening effect taking place at the interface, meaning a decrease in the slip region should have been observed. The reversed behavior at the joint interface may indicate that the frictional and contact properties of the finite element model need to be adjusted.

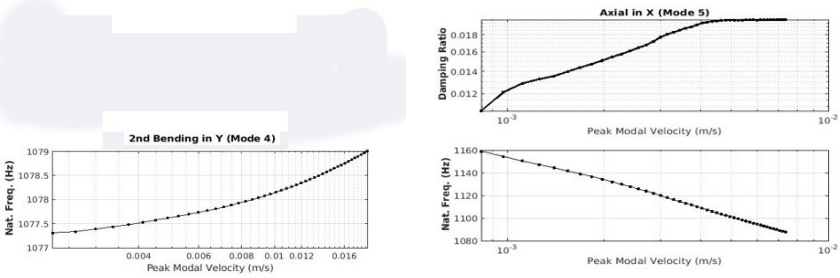

(a) (b)

Fig. 6: Amplitude dependent damping and frequency predicted from the FEM using QSMA for (a) Mode 4 and (b) Mode 5

Despite its acknowledged inconsistency with the experimental results, the QSMA simulations still were utilized as an initial investigation to determine if it could replicate the coupling behavior seen in the experiment. The modal displacement of each mode was tracked as the amplitude of the mode in question increased, in order to examine modal coupling. The modal displacement is an indication of mode activation and hence modal coupling. Each modal displacement was normalized by the mode of interest to compare the activation of all the modes. This results in the displacement ratio parameter, which is the preferred parameter to quantify the degree of modal coupling. Figure 7 show the modal displacement ratio for all six modes with Modes 4 and 5 as the modes of interest.

When Mode 4 is activated during QSMA, Modes 2, 3, and 5 can be seen to respond fairly significantly. The modal displacement ratio for Mode 5 is approximately 7×10^{-2}, which is not as large as that for Modes 2 and 3, but perhaps this is still the most significant coupling considering how close the

natural frequencies are for Modes 4 and 5. As for the other activated modes, the similar mode shapes of the 1st and 2nd bending modes in y may have caused the activation present in Figure 7. Although there have not been experiments to determine any coupling with the torsional mode, the QSMA predicts that some may be present.

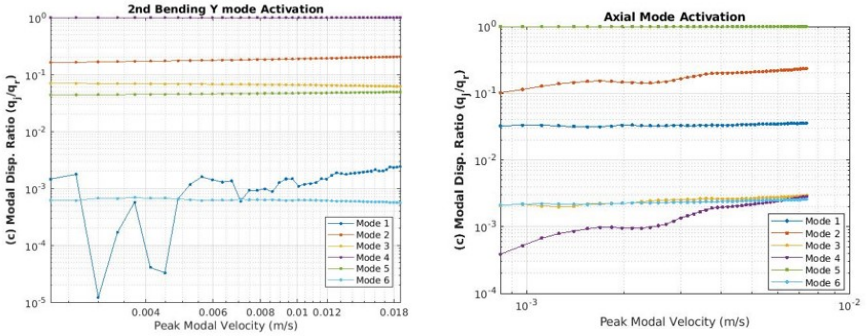

(a) (b)

Fig. 7: Activation of other modes when QSMA is applied to (a) Mode 4 and (b) Mode 5

When Mode 5 is activated, Modes 1 and 2, the 1st bending modes in y and z respectively, are activated most significantly. We expected to see the strongest coupling with Mode 4 (the 2nd bending in y). Again, these phenomena need to be studied further and could potentially be related to the inaccuracies in the QSMA predictions discussed earlier.

5 Nonlinear ROM

A nonlinear ROM was created using a Hurty/Craig-Bampton (HCB) transformation of the KB-AP Assembly, as an additional method to attempt to model the coupling seen in the experiment. The first step in this process is to construct a linear realization (Section 5.1). Next, nonlinear elements can be included in the joint to capture nonlinear response.

5.1 Linear Model Creation for Use in the ROM

In the construction of the model, two fundamental principles were applied:

1. The connectivity of a joint is controlled by the pressure distribution within that joint (see Figure 9), and often joint connectivity on a surface takes the shape of an annular region, and

2. All joint nodes can be tied to a single 6-DOF linear spring joint using rigid RBAR links, which can be used to model the entire joint.

A Sierra/SM simulation was run using a bolt preload of 2000lb_f to determine the outer radius of the annular region. It was ultimately determined that the outer diameter of this annular region would be 1.1". This is a parameter that can be adjusted to tune the model to the linear experimental results.

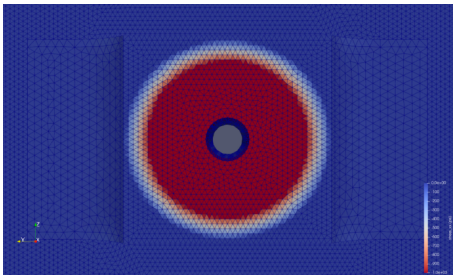

Fig. 8: Contact Pressure Distribution as Calculated in Sierra/SM

A common strategy used in joint modeling is the creation of a simple single 6-DOF spring model to simulate the entire joint using multi-point constraints (MPC). Such a strategy is often implemented by connecting infinitely rigid RBAR links from the interface nodes to a single point. This process is known as "spidering", and an example of it is shown for the S4 Beam in [15]. The location of the spring nodes is typically given to be in the centroid of the bolt, and this strategy was adopted for this work.

The joint model should be mathematically isolated from the rest of the system for this analysis. This was accomplished using the Hurty/Craig-Bampton (HCB) method, which partitions an N DOF system into boundary and internal DOF's.

$$\begin{bmatrix} \mathbf{M}_{ss} & \mathbf{M}_{sb} \\ \mathbf{M}_{bs} & \mathbf{M}_{bb} \end{bmatrix} \begin{bmatrix} \ddot{\mathbf{x}}_s \\ \ddot{\mathbf{x}}_b \end{bmatrix} + \begin{bmatrix} \mathbf{K}_{ss} & \mathbf{K}_{sb} \\ \mathbf{K}_{bs} & \mathbf{K}_{bb} \end{bmatrix} \begin{bmatrix} \mathbf{x}_s \\ \mathbf{x}_b \end{bmatrix} = \begin{bmatrix} \mathbf{f}_s \\ \mathbf{f}_b \end{bmatrix}, \tag{3}$$

where $\mathbf{x}_s \in \mathbb{R}^P$ and $\mathbf{x}_b \in \mathbb{R}^Q$ with $P + Q = N$. In the HCB method, we define the following transformation:

$$\mathbf{x} = \begin{bmatrix} \mathbf{x}_s \\ \mathbf{x}_b \end{bmatrix} = \mathbf{T}_{\text{HCB}} \begin{bmatrix} \mathbf{q}_s \\ \mathbf{x}_b \end{bmatrix}, \qquad \mathbf{T}_{\text{HCB}} = \begin{bmatrix} \mathbf{\Phi}_{\text{fb}} & \mathbf{\Phi}_{\text{c}} \\ \mathbf{0} & \mathbf{I} \end{bmatrix}, \tag{4}$$

where $\mathbf{\Phi}_{fb}$ are the fixed base mode shapes and $\mathbf{\Phi}_{\text{c}}$ are the constraint modes, which are sometimes referred to as boundary node functions. Further discussion of the HCB method may be found in the references [16–19].

Sandia's Rapid Optimization Library (ROL) was then used to find the optimal spring stiffness parameters $\boldsymbol{k}^\star$ which is a 6-DOF spring connecting the two HCB super elements and consists of three translational (lin x, lin y, and

Table 3: Updated $\boldsymbol{k}^\star$ Stiffness Parameters

DOF	lin x	lin y	lin z
Stiffness [lb_f/in]	3.1564×10^6	2.40621×10^6	100.0×10^6
DOF	rot x	rot y	rot z
Stiffness [lb_f/rad]	4.46769×10^6	1.30161×10^6	1.56026×10^6

lin z) and three rotational (rot x, rot y, rot z) stiffnesses. Note that $\boldsymbol{k}^\star$ is used in the creation of $\boldsymbol{K}_{bb}$. The ROL is a gradient-based optimizer which was formulated to solve large scale inverse problems and has been incorporated into Sierra/SD to assist in solving material parameter identification problems. Further discussion of the ROL, its background and its uses are found in references [20, 21].

Table 4: Linear Natural Frequencies in Updated Model Used for HCB Reduction

Mode	Model [Hz]	Experimental (Truth) [Hz]	Error [%]
1^{st} Bending in z	101.614	101.5	-0.112
1^{st} Bending in y	178.890	178.9	0.006
1^{st} Torsion about x	348.076	348.1	0.007
2^{nd} Bending in y	1137.250	1137.3	0.004
1^{st} Axial in x	1182.250	1182.2	-0.004
2^{nd} Bending in z	1458.200	1469.0	0.735
		max|% Error|	0.735
		$\sum$|% Error|/6	0.147

The elements of $\boldsymbol{k}^\star$ were obtained with the optimization routine and are listed in Table 3. The error was then calculated for the first 6 natural frequencies. Table 4 shows that the maximum absolute error obtained is 0.735% and that the 1-norm of the errors is 0.147%. This was deemed acceptably low for this work and highlights the efficacy of this method when one has test data to which the reduced model can be tuned.

After $\boldsymbol{k}^\star$ was found, the full fidelity finite element model was run again with the updated parameters. The tracked nodes with accelerometers were then collected and a mode shape matrix was generated. The experimental and analytical mode shapes were then checked against each other using the MAC [13, 14] in order to verify that the mode shapes in the linearly updated model closely match that from the experiment. This MAC is shown in Figure 9 and shows good agreement between the experimental and FEM mode shapes with $\min_{i\in[1,\ldots,6]} \text{MAC}_{ii} = 0.997$.

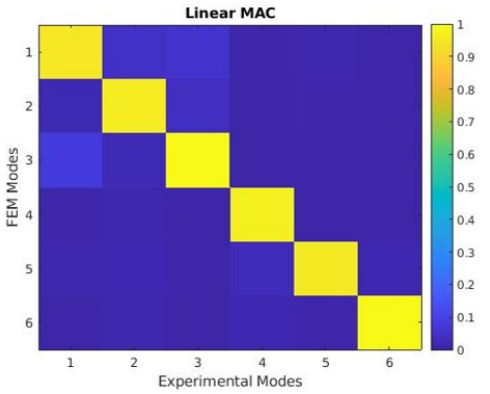

Fig. 9: MAC between mode shapes obtained from the linear FEM model and the experiment

5.2 Nonlinear Model Updating

After the linear stiffness parameters were obtained, the code and method used by [5] were then employed to replace the lin x and rot z linear springs from $\boldsymbol{k}^\star$ with nonlinear Iwan elements. The parameters of these Iwan elements were then optimized per [5] to reproduce the nonlinear behavior of Modes 4 and 5 observed in the experiments as shown in Figure 4. The fits and Iwan spring parameters are shown in Figure 10 and Table 5.

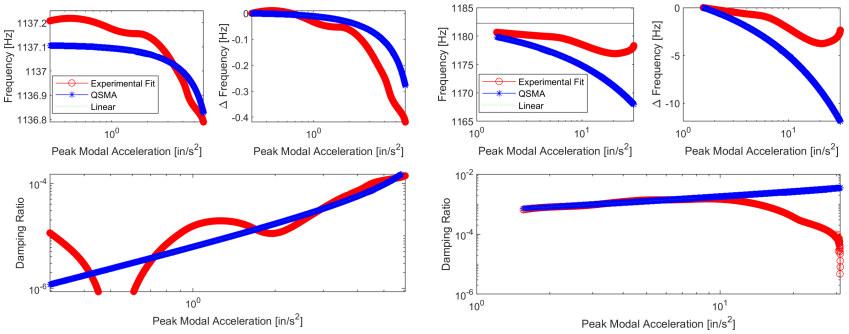

Fig. 10: Nonlinear behavior of the reduced model after tuning to match the experimental measurements for (a) Mode 4 and (b) Mode 5.

As expected, the Iwan spring models Mode 4 fairly well, but perform poorly for Mode 5. This occurs because an Iwan element is comprised of slider elements that are all initially stuck, and so it is not capable of capturing damping that initially decreases. Additionally, the change in the frequency and

Table 5: Iwan Spring Parameters

Mode	F_s	K_T [lb_f/in]	χ	β
rotz	0.1262	12965644	0.3319	0.2494
Mode	F_s	K_T [lb_f/rad]	χ	β
linx	489570	31574600	-0.9849	0.5994

damping of an Iwan element are coupled and so the element is also unable to capture the change in the natural frequency with amplitude. Schedule did not permit a modal coupling study with this model, however this work provides a strong foundation for this to occur as part of future work.

6 Conclusion

This paper has reported on our efforts to apply state of the art test and modeling methods to a structure, which is seemingly simple because it contains only one joint, but proved to be extremely complicated. The bolted joint was found to exhibit both opening/closing and slip. Small imperfections in the actual hardware seem to cause a break in symmetry that is important to its behavior. Given the short (six week) timeframe for this project, significant progress was made in applying both QSMA and nonlinear optimization to model the structure, but issues were encountered that limited the accuracy of the model. For the model updating approach, new physics based constitutive models will be needed that can capture both slip and opening/closing.

The process of quantifying modal coupling using QSMA is a promising and novel concept. However, our effort so far simply confirmed that the model with a symmetric contact surface would not exhibit modal coupling. Because of the challenges that are always encountered when solving contact problems and the fine mesh needed at the interface, six weeks was only adequate to obtain some preliminary QSMA results but not to explore this deeply. Now that this groundwork has been laid, it would be fairly straightforward to explore how changes in the shape of the contact or the friction properties impact modal coupling and this should certainly be pursued.

7 Acknowledgements

Notice: This manuscript has been authored by National Technology and Engineering Solutions of Sandia, LLC. under Contract No. DE-NA0003525 with the U.S. Department of Energy/National Nuclear Security Administration. The United States Government retains and the publisher, by accepting the article for publication, acknowledges that the United States Government retains a non-exclusive, paid-up, irrevocable, world-wide license to publish or

References

[1] Brake, M.: The Mechanics of Jointed Structures: Recent Research and Open Challenges for Developing Predictive Models for Structural Dynamics, (2018). https://doi.org/10.1007/978-3-319-56818-8

[2] Wall, M.P.J., Allen, A. Matthew S, Kuether, R.J.: Observations of Modal Coupling due to Bolted Joints in an Experimental Benchmark Structure. Mechanical Systems and Signal Processing **162**, 107968 (2022). https://doi.org/10.1016/j.ymssp.2021.107968

[3] Sedillo, H., Takeshita, A., Jankowski, K., Barba, J., Bouma, A., Billingsley, E., Abdelkefi, A.: Dynamical analysis on bolted connections of barc structures: numerical and experimental studies. (2021)

[4] Gross, J., Armand, J., Lacayo, R., Reuss, P., Salles, L., Schwingshackl, C., Brake, M., Kuether, R.: A Numerical Round Robin for the Prediction of the Dynamics of Jointed Structures, pp. 195–211 (2016). https://doi.org/10.1007/978-3-319-29763-7_20

[5] Singh, A., Allen, M., Kuether, R.: Spider configurations for models with discrete iwan elements. Mechanical Systems and Signal Processing (Submitted 2021)

[6] Segalman, D.J.: A Four-Parameter Iwan Model for Lap-Type Joints. Journal of Applied Mechanics **72**(5), 752–760 (2005) https://asmedigitalcollection.asme.org/appliedmechanics/article-pdf/72/5/752/5472861/752_1.pdf. https://doi.org/10.1115/1.1989354

[7] Lacayo, R.M., Deaner, B.J., Allen, M.S.: A numerical study on the limitations of modal iwan models for impulsive excitations. Journal of Sound and Vibration **390**, 118–140 (2017). https://doi.org/10.1016/j.jsv.2016.11.038

[8] Lacayo, R.M., Allen, M.S.: Updating Structural Models Containing Nonlinear Iwan Joints Using Quasi-Static Modal Analysis. Mechanical Systems and Signal Processing **118**(1 March 2019), 133–157 (2019). https://doi.org/10.1016/j.ymssp.2018.08.034. Number: 1 March 2019

[9] Khan, M., Hunter, P., Pacini, B., Roettgen, D., Schoenherr, T.: Evaluation of joint modeling techniques using calibration and fatigue assessment of a bolted structure. International Modal Analysis Conference (2020)

[10] A modal model to simulate typical structural dynamics nonlinearity. Proceedings of the 34th International Modal Analysis Conference (2016)

[11] Feldman, M.: Hilbert Transform Applications in Mechanical Vibration, pp. 14–19 (2011)

[12] Singh, A., Allen, M.S., Kuether, R.J.: Multi-mode quasi-static excitation for systems with nonlinear joints. Mechanical Systems and Signal Processing (Submitted May 2021)

[13] Pastor, M., Binda, M., Harčarik, T.: Modal assurance criterion. Procedia Engineering **48**, 543–548 (2012). https://doi.org/10.1016/j.proeng.2012.09.551. Modelling of Mechanical and Mechatronics Systems

[14] Allemang, R.J.: The modal assurance criterion–twenty years of use and abuse. Sound and vibration **37**(8), 14–23 (2003)

[15] Singh, A., Wall, M., Allen, M.S., Kuether, R.J.: Spider configurations for models with discrete iwan elements. In: Kerschen, G., Brake, M.R.W., Renson, L. (eds.) Nonlinear Structures and Systems, Volume 1, pp. 25–38. Springer, Cham (2020)

[16] CRAIG, R.R., BAMPTON, M.C.C.: Coupling of substructures for dynamic analyses. AIAA Journal **6**(7), 1313–1319 (1968) https://doi.org/10.2514/3.4741. https://doi.org/10.2514/3.4741

[17] Roettgen, D., Seeger, B., Tai, W.C., Baek, S., Dossogne, T., Allen, M., Kuether, R., Brake, M.R.W., Mayes, R.: A comparison of reduced order modeling techniques used in dynamic substructuring. In: Allen, M., Mayes, R.L., Rixen, D. (eds.) Dynamics of Coupled Structures, Volume 4, pp. 511–528. Springer, Cham (2016)

[18] Hurty, W.C.: Vibrations of structural systems by component mode synthesis. Transactions of the American Society of Civil Engineers **126**(1), 157–175 (1961) https://ascelibrary.org/doi/pdf/10.1061/TACEAT.0008073. https://doi.org/10.1061/TACEAT.0008073

[19] Young, J., Haile, W.: Primer on the craig-bampton method (2000)

[20] Bunting, G., Miller, S.T., Walsh, T.F., Dohrmann, C.R., Aquino, W.: Novel strategies for modal-based structural material identification. Mechanical Systems & Signal Processing **149**, (2021)

[21] Bunting, G.: Strong and weak scaling of the sierra/sd eigenvector problem to a billion degrees of freedom. (2019). https://doi.org/10.2172/1494162

Appendix

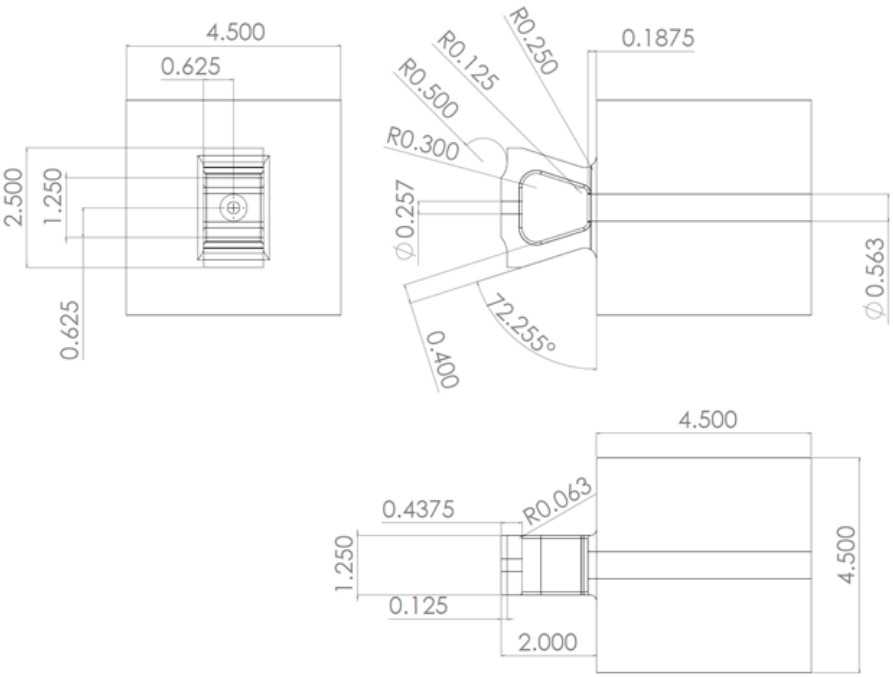

Fig. 11: KB Dimensioned Drawing

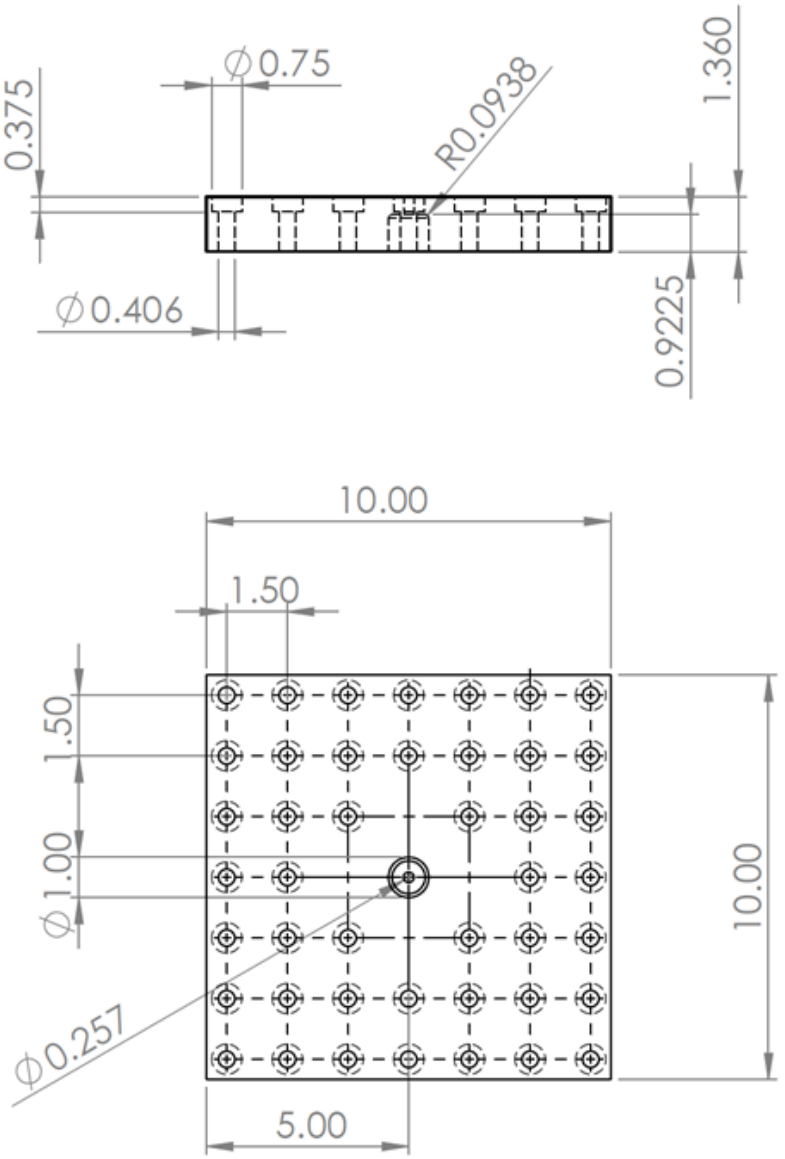

Fig. 12: AP dimensioned shop drawing